Geomechanics for Energy and the Environment 43 (2025) 100733

Contents lists available at ScienceDirect

Geomechanics for Energy and the Environment

journal homepage: www.elsevier.com/locate/gete

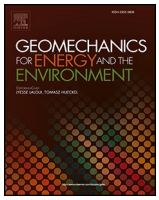

Numerical comparison between square and circular plate anchors in clay

Mohammadreza Jahanshahinowkandeh, Marina Miranda, Jorge Castro *

Department of Ground Engineering and Materials Science, Universidad de Cantabria, ETSI Caminos, Canales y Puertos, Avda. de los Castros s/n, Santander, Spain

ARTICLE INFO

Keywords:
Plate anchors
Pullout
Clay
FELA
Shape
Failure
Spacing

ABSTRACT

This paper presents a numerical comparison of the vertical pull-out capacity of square and circular anchors in purely cohesive soils (i.e. clays in undrained conditions). For simplicity, ultrathin, infinitely rigid anchors are considered and to isolate the effect of anchor shape, comparisons are made between anchors of equal area and embedment depth. Finite Element Limit Analyses (FELA) are used to compute upper and lower bound values of the break-out factor over the full range of embedment ratios, and the associated failure mechanisms are identified. The results show for the first time (to the best of the authors' knowledge) that square anchors exhibit slightly higher efficiency at shallow embedment ratios due to their larger perimeter, while at greater depths, circular anchors become more efficient as a result of the different failure mechanisms involved. The study also investigates the influence of anchor inclination and shows that inclined anchors have a higher pull-out capacity in vented conditions due to elongated failure mechanisms. Under attached conditions, the deep failure mechanism is obtained in most cases with the corresponding constant break-out factor. In addition, the paper analyses the influence of anchor spacing in anchor groups, identifying optimal spacing to avoid capacity reduction due to interaction effects. For shallow depths, a spacing of about two times the anchor width is sufficient, while deeper installations require larger spacings due to the extended failure zone. Once the deep failure mechanism is reached, spacing requirements decrease again, less than two times the anchor width. Overall, the presented numerical simulations offer insights for the design of plate anchors in cohesive soils, contributing to the advancement of offshore foundation technologies.

1. Introduction

Offshore renewable energy technologies play a key role in achieving carbon reduction targets, particularly in Europe, where offshore wind energy resources are abundant. Most of these resources lie in waters deeper than 60 m, where bottom-fixed solutions are currently not economically competitive (e.g.,[24]). Thus, floating solutions can extend wind power into new deep-water areas, though these pose technical challenges, for example, for mooring lines and anchoring systems, whose cost increases with depth.

In deeper waters, taut mooring systems or Tension Leg Platforms (e.g.,[2]), widely used in the oil & gas industry, become attractive due to their reduced footprint and line length. These systems require anchors capable of withstanding high inclined loads, such as suction caissons and plates (e.g.,[23]), where bearing resistance dominates over frictional resistance.

Plate anchors are a well-established anchoring solution and the development of new or existing keying processes, such as suction embedded plate anchors (SEPLA) (e.g.,[7]), dynamically embedded plate anchors (DEPLA) (e.g.,[6,20,9]) or gravity installed plate anchors (GIPLA) (e.g.,[13]), are encouraging their adoption. For practical purposes, circular, square, rhomboid and rectangular anchors (e.g.,[8]) may be considered. Recently, more complex shapes, such as biwing anchors[5], have also come under consideration. Plate anchor behaviour has been studied theoretically (e.g.,[26]), experimentally (e.g.,[4]) and numerically (e.g.,[18]), with ongoing research addressing cyclic loading (e.g.,[3]), consolidation (e.g.,[12,28]) and non-uniform soil properties (e.g.,[10]). Here, the main focus is on comparing the pull-out capacity of circular and square anchors in clay for an idealised case, namely ultrathin and infinitely rigid anchors.

One of the first detailed comparisons between circular and square plate anchors, but in sand, was by Ovesen[22] using centrifuge tests. He found similar uplift capacities when both anchors have the same embedment depth and area. Ovesen[22] also analysed a circular anchor with a diameter equal to the side of the square anchor ($B=D$), finding lower total pull-out capacity for circular plates but higher dimensionless capacity (pull-out factor) due to deeper relative embedment. Murray

* Correspondence to: Group of Geotechnical Engineering, Department of Ground Engineering and Materials Science, Universidad de Cantabria, Avda. de los Castros s/n, Santander 39005, Spain.

E-mail addresses: mreza.jahanshahi@unican.es (M. Jahanshahinowkandeh), mirandama@unican.es (M. Miranda), castrogj@unican.es (J. Castro).

https://doi.org/10.1016/j.gete.2025.100733
Received 10 April 2025; Received in revised form 16 July 2025; Accepted 21 August 2025
Available online 23 August 2025

NOTATION

A	Anchor area
B	Anchor side width
c_u	Undrained shear strength
D	Anchor diameter
E_u	Undrained Young's modulus
H	Anchor embedment
K_0	At-rest earth pressure coefficient
N_c	Break-out factor
N_{c0}	Break-out factor for weightless conditions
N^*_{c0}	Maximum break-out factor
n	Spacing ratio
Q	Pull-out capacity
q	Surface surcharge
z	Vertical distance from the ground surface
θ	Anchor inclination
γ'	Effective unit weight
ν_u	Undrained Poisson's ratio
Δ	Soil displacement
Δ_{max}	Maximum soil displacement

and Geddes[19] found the break-out factor for circular plates to be about 1.26 times that for square plates (B=D), consistent with Merifield et al.[16], who theoretically estimated it as $4/\pi \approx 1.27$ for deep cases. For shallower cases, this ratio decreases[16].

Comparisons in cohesive soils are more limited. Das[4] presented a general comparison of square and circular plates in clay using 1 g laboratory results. Martin and Randolph[15] derived the exact solution for the deep failure mechanism of circular anchors (namely, a break-out factor of 13.11 for rough anchors and $3(\pi+1) \approx 12.42$ for smooth ones), but no exact solution has been presented for square anchors due to the tridimensionality of the problem. Merifield et al.[17] found, using lower bound FELA and considering B=D, that the break-out factor for circular plates is slightly larger than for square plates (with maximum differences up to around 15 % for H/B=2). Finally, Wang et al.[27] compared square and circular anchors using finite element analyses, but their results are influenced by the mesh and the anchor thickness.

This manuscript demonstrates, for the first time to the authors' knowledge, that when anchors of equal area and embedment depth are compared, square anchors are more efficient at very shallow depths due to their larger perimeter, whereas circular anchors become more efficient at greater depths owing to their favourable deep failure mechanism. To date, some authors[17,27] have attributed the superior performance of circular anchors in terms of the break-out factors at shallow depths to their shape; however, it is shown here that this is caused by the assumption of $B = D$. Furthermore, a detailed numerical characterisation of the deep failure mechanism for square anchors is presented here for the first time. In addition, this study provides new insights into the effects of anchor inclination and optimal spacing within anchor groups. In the following, Section 2 defines the problem under study, Section 3 presents the numerical models used and next, the corresponding numerical results are summarised and discussed in Section 4. Finally, some conclusions are derived.

2. Problem definition

Here, idealised cases of ultrathin and infinitely rigid plate anchors embedded in a homogeneous rigid-plastic Tresca material (i.e., with uniform undrained shear strength, c_u, and very high stiffness, E_u) are considered. Installation effects are not considered. The soil is allowed to develop tensile stresses freely, except usually at the bottom of the anchor, where a null stress (immediate breakaway or vented conditions) is imposed. For comparison, some additional cases with attached conditions (allowing suction beneath the anchor) are also analysed. Unlike strip anchors, the capacity of circular and square plate anchors is influenced by the surface roughness. Here, anchors are assumed to be perfectly rough, but not all the shear resistance is mobilised[15].

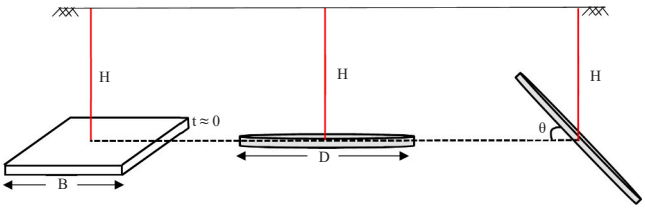

Fig. 1. Schematic display of the embedded anchors in saturated clay.

The variables of this problem (Fig. 1) are as follows:

(a) Geometrical variables: anchor area (A); anchor diameter (D) for circular anchors or anchor side width (B) for square ones; anchor embedment (H), anchor thickness, assumed as null here ($t \approx 0$) and anchor inclination (θ), initially set to 90° (i.e. horizontal anchor) (Fig. 1).
(b) Boundary condition beneath the anchor: vented conditions (immediate breakaway) are generally considered, except in specific analyses where attached conditions are included.
(c) Initial stress state: γ', K_0. Several authors[25,27] suggest using the buoyant unit weight because hydrostatic pressures appear beneath the anchor when the soil is fully submerged and free water gets beneath the anchor. For the pull-out capacity using limit analysis, K_0 does not have any influence and, using a dimensional analysis, only the weightless case (γ=0) needs to be analysed.
(d) Surface surcharge at the seabed, easily included but disregarded here for simplicity (q=0).
(e) Soil properties: stiffness (ν_u=0.5, E_u) and strength (c_u).
(f) Anchor properties: assumed as infinitely stiff and as infinitely rough.
(g) Results, e.g. pull-out capacity (Q).

Focusing on the pull-out capacity (Q) and disregarding the soil displacements (i.e., infinitely rigid soil, limit strength problem), its value may be expressed in a dimensionless analytical manner as:

$$\frac{Q}{Ac_u} = N_c = N_{c0} + \frac{\gamma' H}{c_u} \le N^*_{c0} \tag{1}$$

where N_c and N_{c0} are the break-out factor and the break-out factor for weightless conditions (γ'=0), respectively. Consequently, the study here focuses on N_c and N_{c0} values. N^*_{c0} is the maximum value corresponding to the deep failure mechanism.

Merifield et al.[17] and other authors compared square and circular anchors by equating the side width of the square anchor to the diameter of the circular anchor (B=D). Here, for the sake of rigour and because the pull-out force of the anchor is mainly controlled by its embedment depth and area, the comparison between square and circular anchors is performed by equating their areas:

$$A = B^2 = \frac{\pi}{4} D^2 \tag{2}$$

Then, the diameter of the circular anchors is chosen so that the area of both anchor shapes is the same:

$$D = \frac{2B}{\sqrt{\pi}} \tag{3}$$

The comparison must also be made for the same embedment depth (H). Here, H is made dimensionless using $\sqrt{A}$:

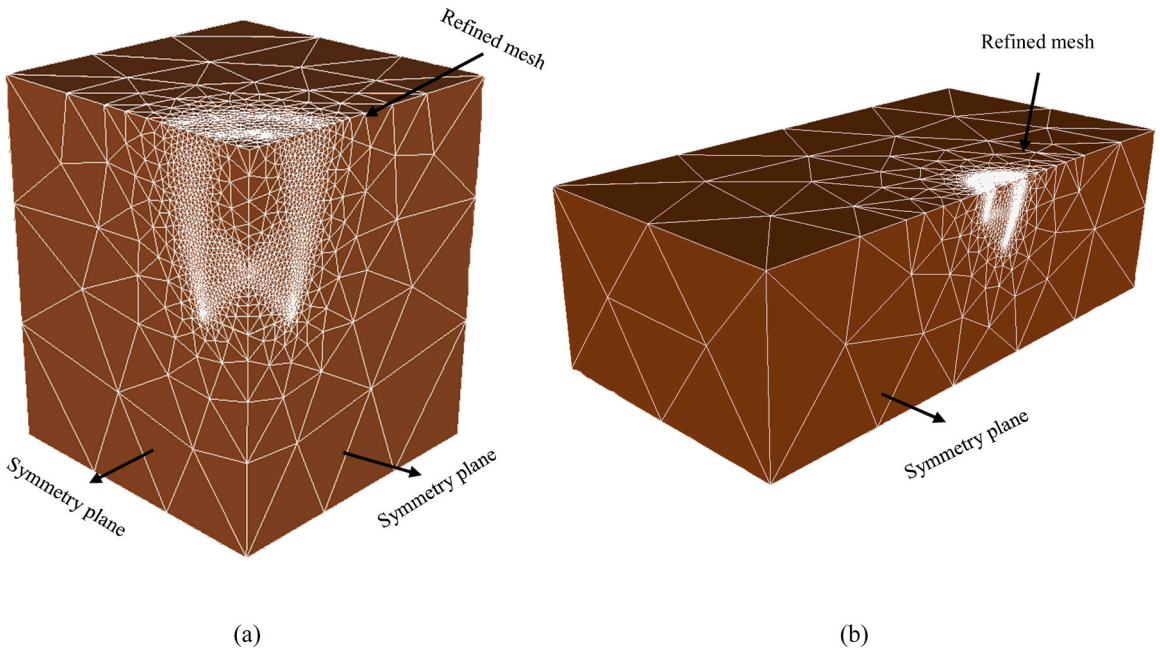

Fig. 2. Typical meshes of numerical models with adaptivity after calculation: (a) horizontal anchor; (b) inclined anchor.

Table 1
Mesh sensitivity analysis of simulations.

Number of elements	10,000	20,000	40,000	60,000	80,000
Break-out factor	9.98	9.78	9.66	9.61	9.58

$$\frac{H}{\sqrt{A}} = \frac{H}{B} = \frac{2}{\sqrt{\pi}}\frac{H}{D} \tag{4}$$

3. Numerical models

This section describes the numerical models used to investigate the pull-out force of circular and square anchors. Finite element limit analyses (FELA) were performed using OPTUM 3 G[21] to obtain upper and lower bound values (UB & LB).

The anchor is modelled as "wished-in-place" (i.e., neglecting installation effects) and as an infinitely thin rigid plate with no thickness and interfaces on both sides. In the vented condition (immediate breakaway), the interfaces were modelled with the same properties as the soil plus a tension cut-off, allowing separation from the soil. However, in the attached condition, this was not considered. The adhesion of these interfaces was set equal to c_u to reproduce a perfectly rough contact. The vertical pull-out force is applied as a uniformly distributed vertical stress on the surface of the anchor. The analysis is done in undrained conditions.

The employed FELA code allows for adaptive mesh refinement, which enables the creation of initial models using fewer elements and automatic mesh refinement during calculation in areas of interest. This process enhances result precision while simultaneously reducing computational costs. Fig. 2 shows a typical mesh of the numerical model used in this study. As shown in Fig. 2, because the size of the inclined anchors was larger than the horizontal ones, the number of adaptivity

Table 2
FELA break-out factors for different embedment ratios of circular and square anchors.

H/B	*H/D*	N_{c0} Circular (UB)	N_{c0} Circular (LB)	N_{c0} Square (UB)	N_{c0} Square (LB)	Circular/Square (UB)	Circular/Square (LB)
0.2	0.18	0.73	0.7	0.8	0.76	0.92	0.91
0.4	0.35	1.47	1.41	1.58	1.54	0.93	0.91
0.6	0.53	2.27	2.12	2.48	2.27	0.92	0.93
0.8	0.71	2.99	2.83	3.15	2.99	0.95	0.95
1	0.89	3.73	3.53	3.96	3.71	0.94	0.95
1.3	1.15	4.76	4.58	4.95	4.69	0.96	0.98
1.5	1.33	5.46	5.25	5.57	5.28	0.98	0.99
1.7	1.51	6.11	5.84	6.19	5.85	0.99	1.00
2	1.77	6.85	6.61	6.96	6.62	0.98	1.00
2.3	2.04	7.59	7.28	7.65	7.25	0.99	1.00
2.5	2.22	7.99	7.68	8.08	7.64	0.99	1.01
3	2.66	8.88	8.54	8.92	8.50	1.00	1.00
3.5	3.10	9.64	9.27	9.66	9.24	1.00	1.00
4	3.54	10.20	9.89	10.24	9.83	1.00	1.01
4.5	3.99	10.83	10.42	10.87	10.37	1.00	1.00
5	4.43	11.26	10.91	11.36	10.86	0.99	1.00
6	5.32	12.14	11.70	12.18	11.65	1.00	1.00
7	6.20	12.83	12.33	12.62	12.12	1.02	1.02
8	7.09	13.08	12.64	12.77	12.25	1.02	1.03
9	7.98	13.32	12.80	12.80	12.26	1.04	1.04
10	8.86	13.33	12.80	12.80	12.27	1.04	1.04

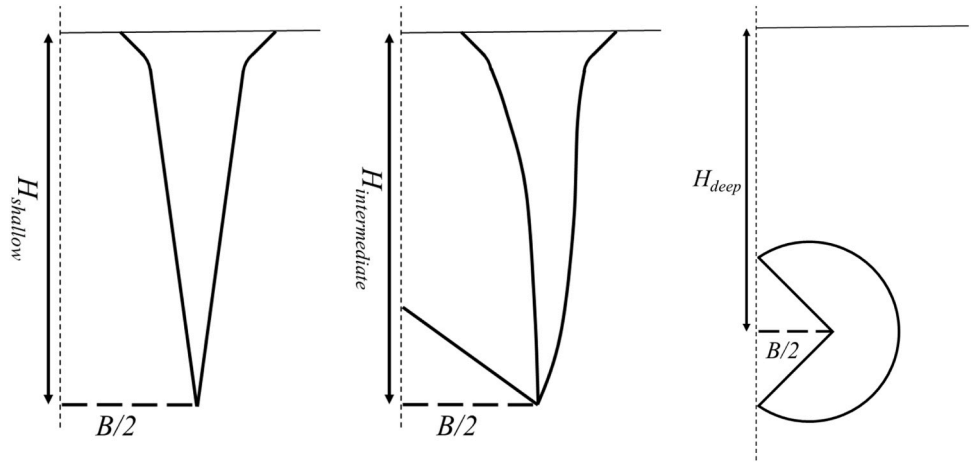

Fig. 3. Schematic view of the very shallow, intermediate and deep failure mechanisms.

used for them was 8. However, the results showed a good accuracy for horizontal cases with an adaptivity number of 6. In order to achieve fine meshes around the anchors, the number of elements for horizontal and inclined cases was respectively set to 40,000 and 60,000, as shown in Fig. 2. Table 1 shows the mesh sensitivity analysis of a randomly chosen model in this study (UB, horizontal, square, H/B=3.5). As seen, the difference between two consecutive models becomes less than 1 % when the number of finite elements is 40,000 or more.

As can be seen in Fig. 2, only a quarter of the model was simulated for the horizontal anchors, whereas half of the model was simulated for the inclined anchors. The boundary conditions at the bottom of the models were fixed in all directions, while the symmetry planes were fixed only in the direction perpendicular to the specified symmetry plane. In addition, the sides of the models were only free in the vertical direction. The model size was chosen large enough to avoid boundary effects, based on sensitivity analyses for different embedment depths. For shallow models, the lateral width ranged from 3.3B (horizontal) to 6.6B (inclined), increasing up to 11.3B and 16B for deep cases. Soil depth below the anchor was 2.3B and 3.3B, respectively, considered conservative to prevent boundary influence under attached conditions.

The soil is assumed to be an elastic-perfectly plastic Tresca material. The following parameters were used for the soil: $c_u = 50$ kPa, $\nu_u = 0.5$, and $E_u = 1 \times 10^6$ MPa. The unit weight of the soil is initially assumed as zero (γ=0) to obtain weightless break-out factors (N_{c0}). Later, cases with unit weight (γ'=10 kN/m^3) were analysed to assess the transition to deep failure mechanisms.

A square anchor width of B= 1.5 m was chosen to generate the geometric model, although its specific value does not affect the dimensionless results (N_c and N_{c0}). According to Eq. (3), the circular anchor has a diameter of D= 1.69 m. Different embedment ratios (i.e., H/B) ranging from 0.2 up to 10 in weightless soil were modelled (Table 2). In order to study the effect of the unit weight of the soil and the attachment of the anchor surface to the underlying soil (i.e., no breakaway condition), some cases with different embedment ratios increasing from 1 to 10 were also modelled. Finally, to evaluate the effect of θ on the break-out capacity, two inclined cases (θ =45° and 90°) were modelled under weightless, weighted soil and attached condition.

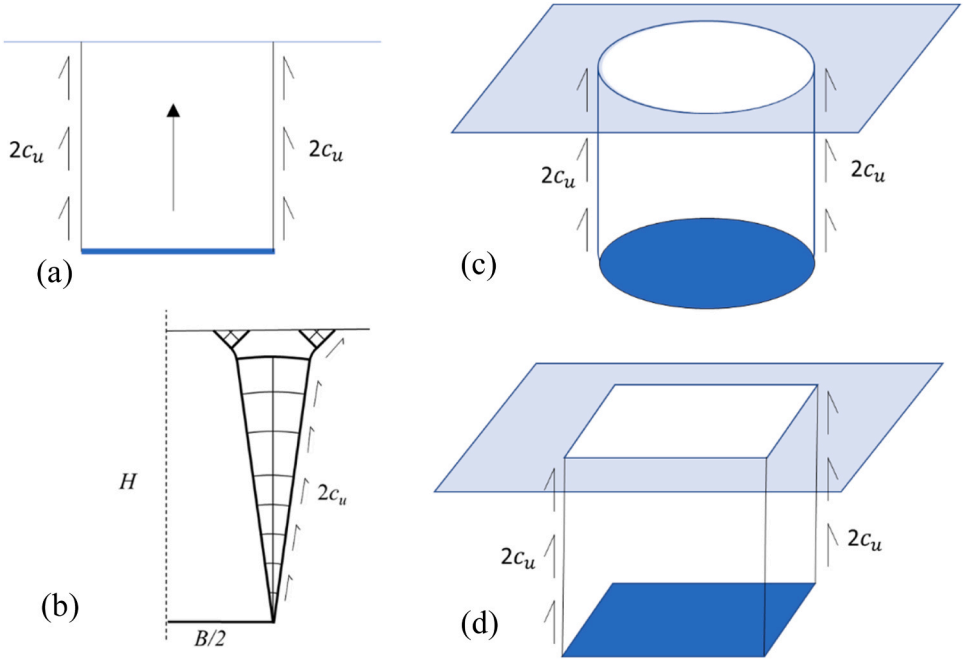

Fig. 4. Very shallow failure mechanisms: (a) Vertical kinematic mechanism for strip anchor; (b) Exact characteristic lines for strip anchor (after[14]); (c) Vertical kinematic mechanism for circular anchor; (d) Vertical kinematic mechanism for square anchor.

Table 3
Break-out factors for circular and square anchors for very shallow conditions: comparison between analytical and numerical methods.

	N_{c0} Circular			N_{c0} Square		
H/√A	FELA (UB)	Analytical (UB)	FELA (LB)	FELA (UB)	Analytical (UB)	FELA (LB)
0.2	0.73	0.71	0.7	0.8	0.8	0.76
0.4	1.47	1.42	1.41	1.58	1.6	1.54
0.6	2.27	2.13	2.12	2.48	2.4	2.27
0.8	2.99	2.84	2.83	3.15	3.2	2.99
1	3.73	3.54	3.53	3.96	4	3.71
1.3	4.76	4.61	4.58	4.95	5.2	4.69
1.5	5.46	5.32	5.25	5.57	6	5.28
1.7	6.11	6.03	5.84	6.19	6.8	5.85
2	6.85	7.09	6.61	6.96	8	6.62

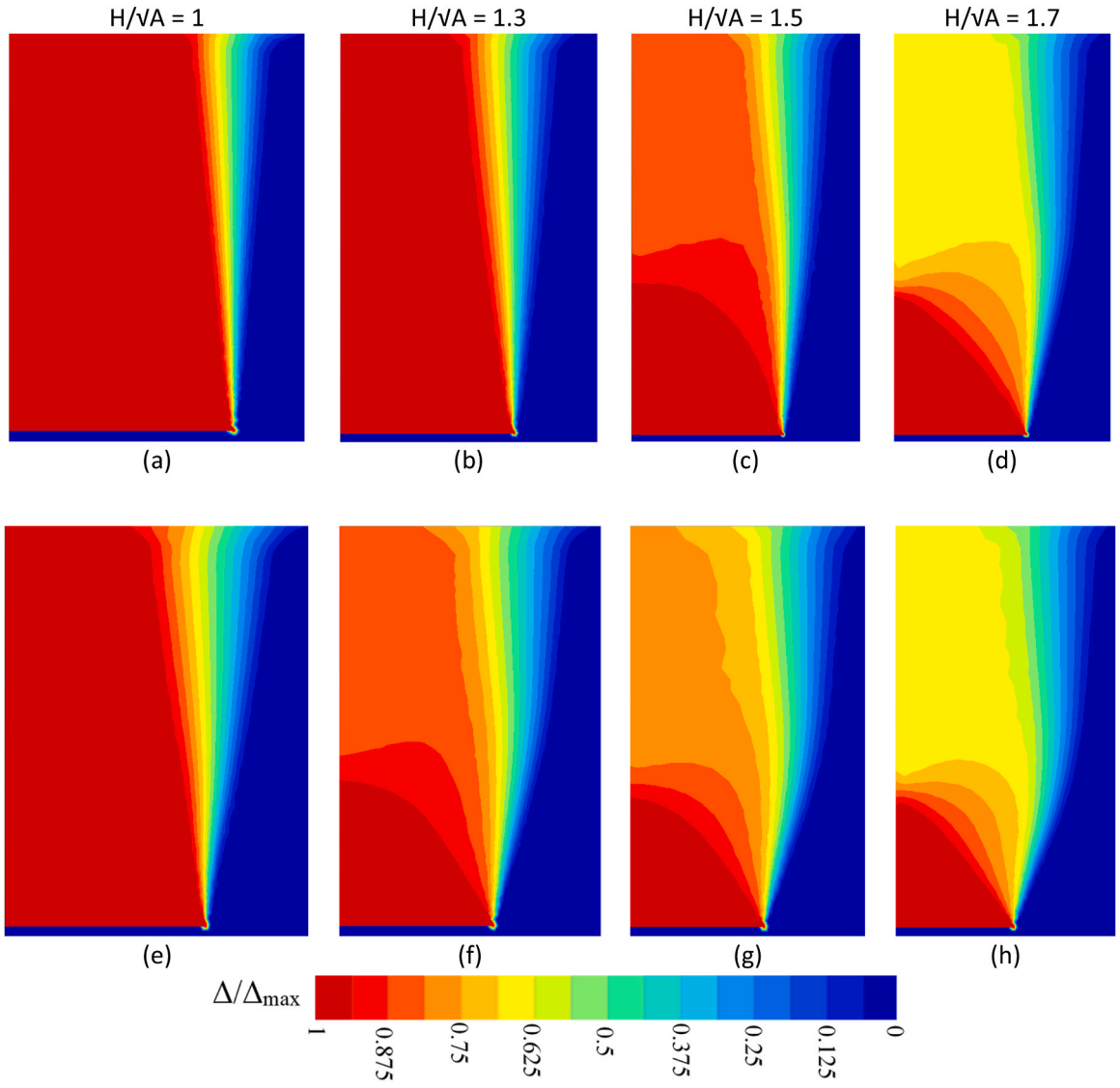

Fig. 5. Displacement contours of anchors with shallow embedment ratios in vertical section (elevation): (a)(b)(c)(d) circular anchor; (e)(f)(g)(h) square anchor.

4. Results and discussion

4.1. Comparison between circular and square anchors

Table 2 summarises the UB and LB values for vertical pull-out. The small differences between UB and LB values (generally <5 %) demonstrate high numerical accuracy, improving upon existing studies. The ratio between the values for circular and square anchors varies from around 0.91 for very shallow cases up to 1.04 for deep cases. As seen in Fig. 3, in a similar manner to strip anchors (e.g.,[1]), three different depths may be distinguished for circular and square anchors, namely: (i) very shallow cases, where the failure mechanism is nearly vertical and constant for circular anchors, and therefore, the break-out factor increases in a linear manner with the embedment depth; (ii) intermediate cases, where a stagnant zone (passive wedge) appears above the anchor and the failure mechanism reaches the surface, but increasing its horizontal extension with the anchor depth; and (iii) deep cases, where the break-out factor reaches a constant value because the failure mechanism

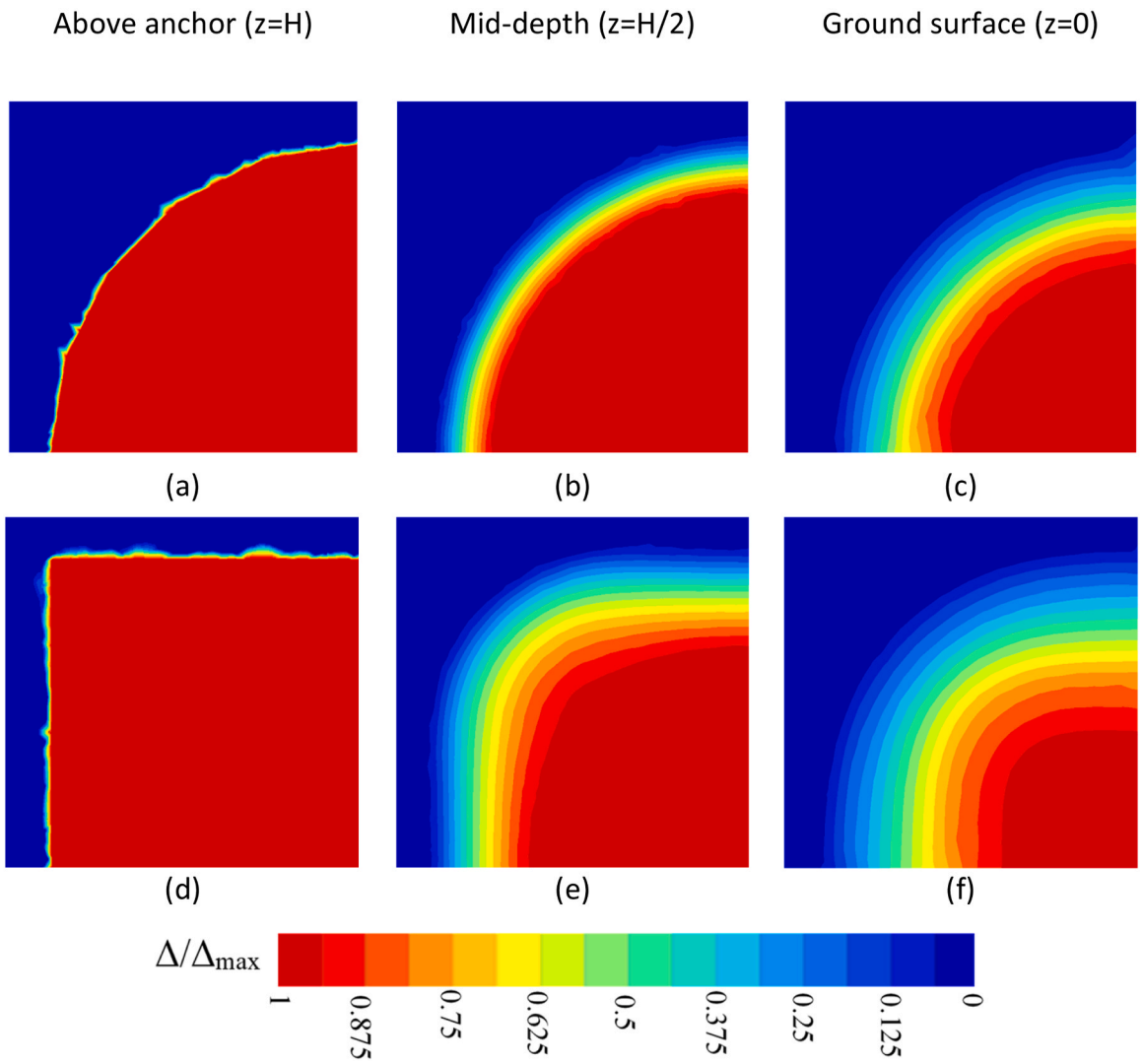

Fig. 6. Horizontal section (plan) views of displacement contours of anchors with embedment ratio of $H/B = 1$ at different levels from ground surface: (a)(b)(c) circular anchor; (d)(e)(f) square anchor.

does not reach the ground surface. In the following, the two limit cases (very shallow and deep) are analysed in detail.

4.1.1. Very shallow failure

For very shallow cases, the vertical kinematic mechanism provides a fairly approximate upper bound solution. For example, for strip anchors, the upper bound solution is $N_{c0}= 2\ H/B$, while the exact solution is $N_{c0}= 1.956\ H/B$[14], resulting in only a 2 % overestimation. The vertical mechanism (Fig. 4a) is not exact because the characteristic lines (slip lines) should reach the ground surface at an angle of 45°. To fulfil this, three plastic regions are formed (Fig. 4b): two small triangular passive regions near the surface and a centred fan at the anchor edge (in half of the model due to symmetry). The break-out factor increases linearly with the embedment depth because the failure mechanism maintains a constant shape. This exact very shallow mechanism provides reasonable values for $H/B< 2$, but it is strictly valid only for $H/B\leq 1.314$[1] when a passive wedge forms above the anchor and the fans are no longer centred at the anchor edge and are not vertically straight.

For circular anchors, the vertical kinematic mechanism (cylinder in Fig. 4c) gives an UB value of N_{c0} equal to 4 times the embedment ratio:

$$N_{c0} = 4\frac{H}{D} \tag{5}$$

These analytical values improve the numerically simulated ones and are very close to the numerical LB values (Table 3), and consequently to the exact solution. The failure mechanism observed using FELA is also formed by two triangles, as for the strip anchor, but in this case, due to axial symmetry, the internal triangle is smaller than the outer one (Fig. 5a and b). The failure mechanism also comprises a vertical fan that starts from the anchor perimeter but has a slight average inclination towards the anchor centre (Fig. 5a and b). This very shallow failure mechanism is valid for $H/\sqrt{A}= 1.3$ or $H/D= 1.15$ (Fig. 5b), but not for $H/\sqrt{A}= 1.5$ or $H/D= 1.33$ (Fig. 5b), where the passive wedge above the anchor starts to appear.

On the other hand, for square anchors, the vertical kinematic mechanism (square prism in Fig. 5d) also gives an UB value of N_{c0} equal to 4 times the embedment ratio:

$$N_{c0} = 4\frac{H}{B} \tag{6}$$

This analytical UB solution quickly loses accuracy with depth (Table 3) because the failure mechanism for the square anchor rapidly transforms from a square cross-section to a circular one (in agreement with the principle of minimum energy) (Fig. 6d, e, f). The rounding of failure mechanisms has also been observed in the laboratory (e.g.,[8]). The formation of a stagnant zone (passive wedge) above the anchor is

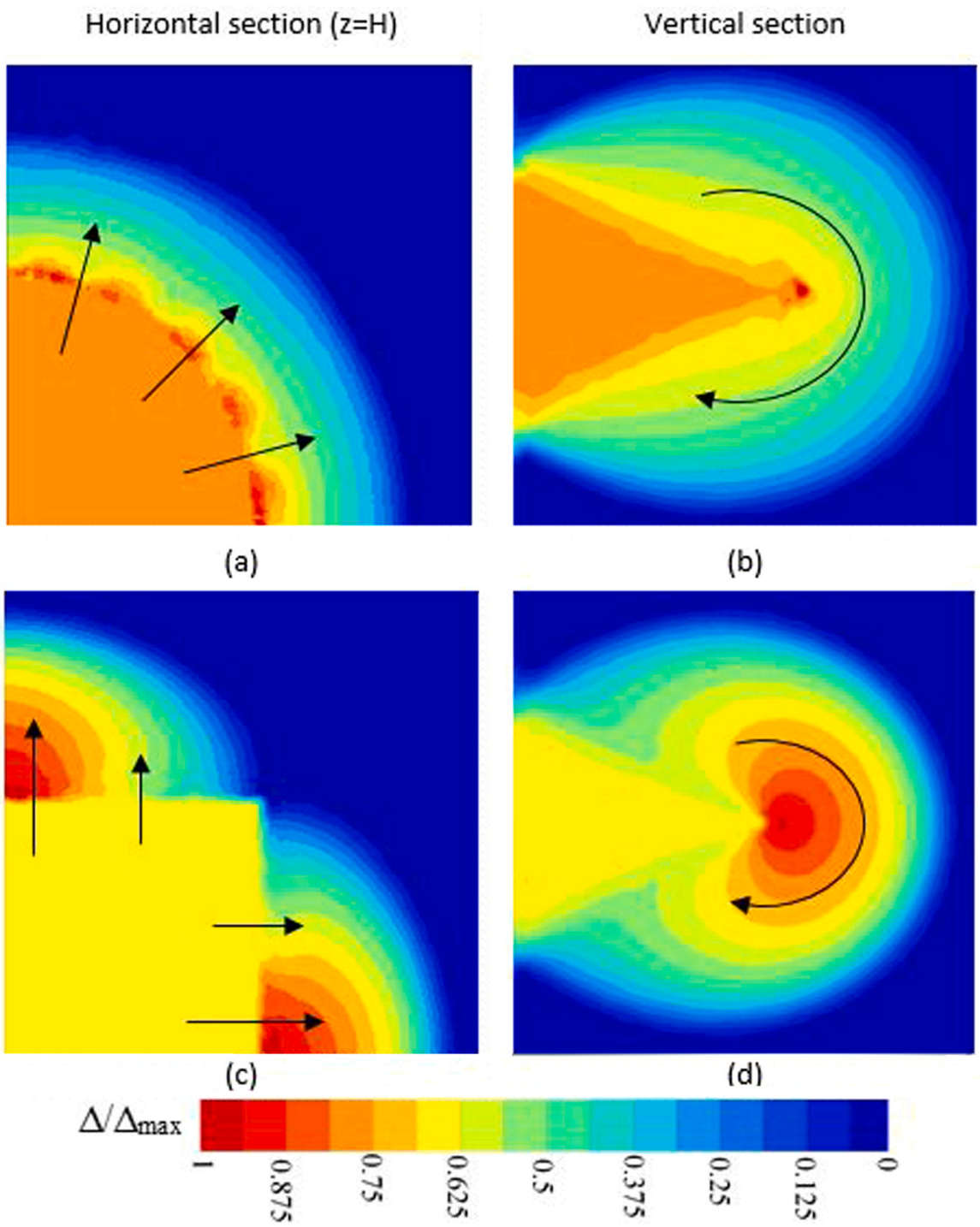

Fig. 7. Horizontal and vertical section views of displacement contours of anchors with embedment ratio of $H/B = 10$: (a)(b) circular anchor; (c)(d) square anchor (arrows indicate soil displacement direction).

observed earlier for square anchors in the numerical simulations, i.e., it is visible for H/B= 1.3 (Fig. 5f).

The FELA values and the UB analytical ones (Tables 2 and 3) show that square anchors are more efficient (per anchor area) at very shallow depths because of their larger perimeter than that of circular ones. The UB analytical solutions (Eqs. 5 and 6) give a circular to square ratio of 0.89 (equal to the perimeter ratio), which could be considered an ideal lowest ratio for an extremely shallow case. The FELA give a ratio of 0.91–0.92 for H/B= 0.2, and it increases with depth (Table 2), as the square failure mechanism gets more rounded and therefore, more similar to the circular one.

4.1.2. *Deep failure*

The presented FELA results (Table 2) provide a maximum value of N^*_{c0}= 12.27–12.80 for square anchors, while they properly bracket (12.80–13.33) the exact solution for the deep failure of circular anchors (13.11)[15]. Thus, contrary to very shallow cases, circular anchors are more efficient (per anchor area) for deep cases, with a circular to square ratio of 1.04 (Table 2). The deep failure mechanism in weightless cases is reached for H/B= 8–9 and slightly earlier for square anchors (Table 2).

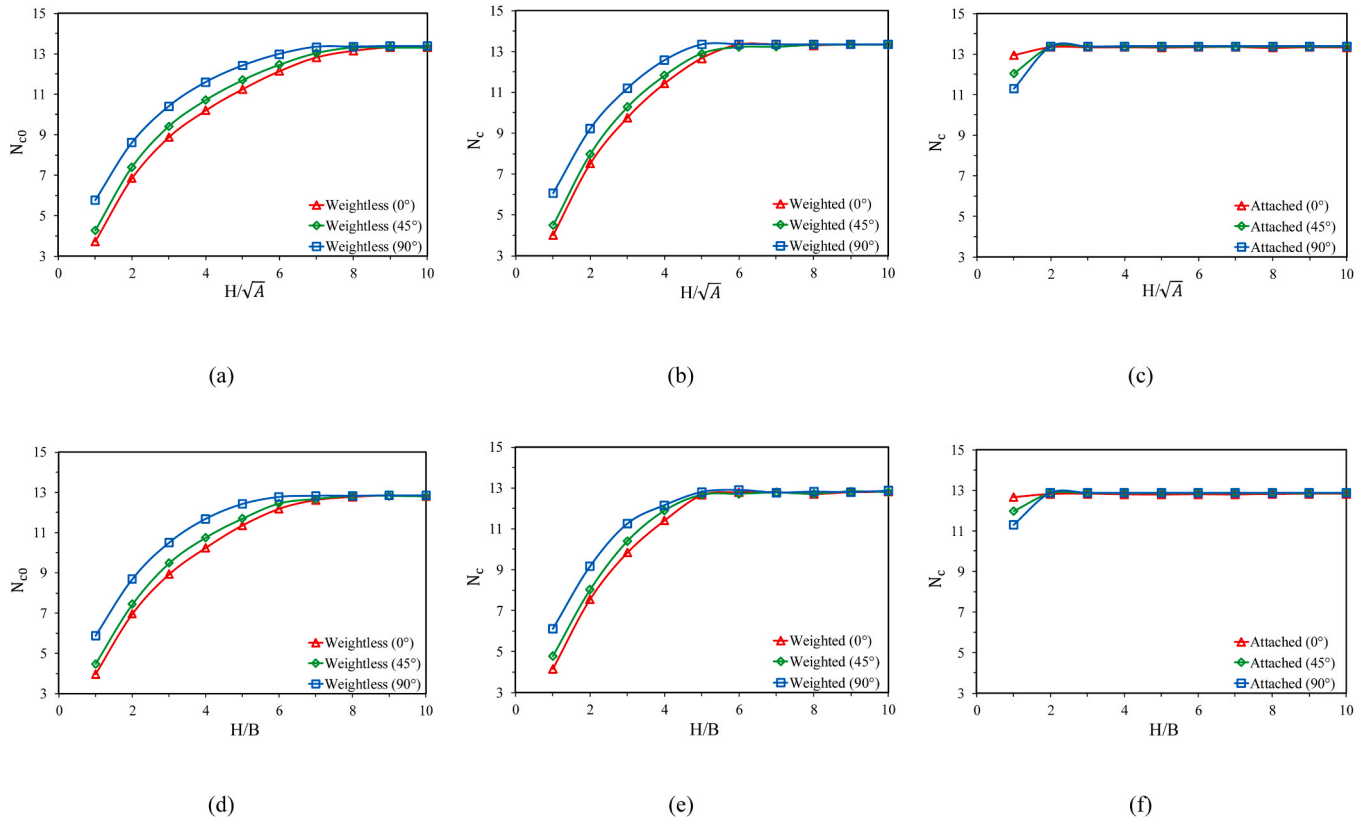

Fig. 8. Upper bound break-out factors of anchors with different inclination angles: (a)(b)(c) circular anchor; (d)(e)(f) square anchor.

In real cases with soil weight, it is reached at shallower depths according to Eq. (1).

Deep failure mechanisms of circular and square anchors (Fig. 7) explain the slightly larger maximum break-out factor of circular anchors. For deep cases, two stagnant zones are formed above and below the anchor and outside them, the soil displaces around the anchor as this is pulled up (Fig. 3c). For circular anchors, the stagnant zones are similar to parabolic cones and for square anchors they are similar to prisms (Fig. 7). For square anchors, the soil does not move symmetrically downward around a central axis, as with circular anchors. Instead, the soil is displaced laterally towards the sides (arrows in Fig. 7c), resulting in a shorter sliding surface and lower mobilised resistance. On the other hand, for circular anchors, the soil displaces in an axially symmetrical manner (arrows in Fig. 7a). Please, note that some slight oscillations at the perimeter of the circular anchor are visible due to minor numerical inaccuracies. In conclusion, the failure mechanisms (Fig. 7) justify the slightly superior performance of circular anchors for deep cases.

4.2. Anchor inclination

4.2.1. Break-out factor

Fig. 8 compares the effect of the inclination of anchors on their break-out factor for vented and attached conditions. The applied load was assumed to be perpendicular to the anchors. As seen, the inclination of the anchors increased their pull-out capacity at the same depth, mostly in vented condition, because it increases the contour (length) of the failure mechanism. Up to the maximum value of the break-out factor (N^*_{c0}) (deep failure), the more the anchor is inclined, the higher its break-out factor becomes. The deep failure mechanism is reached for embedment ratios of 8 and 7 in weightless soil and 6 and 5 in weighted soil (γ'=10 kN/m^3) for circular and square anchors, respectively. The highest observed difference for vertical and horizontal anchors was about 35 % and 32 % in weightless soil for the circular and square anchors, respectively (Fig. 8). Similar to the findings in this study, Jesmani et al.[11] observed that plate anchors exhibited their maximum pull-out capacity when positioned vertically and their minimum capacity when placed horizontally at a specific embedment ratio. Furthermore, the ratio between these two capacities is equal to 1 when the deep failure is reached.

For both types of anchor with attached conditions (Fig. 8c, f), small differences between the break-out factor of the horizontal ($\theta = 0°$) and inclined anchors ($\theta = 45°$ and 90°) are only observed for the embedment ratio of 1, and the deep failure mechanism is computed for larger depths. The pull-out capacity of the anchors with the highest inclination is the lowest at an embedment ratio of 1. At this embedment ratio, the difference between the N_c of the horizontal and vertical anchors is about 14.5 % and 12 % for the circular and square anchors, respectively. This is attributed to the larger length of the shear zone for the horizontal anchor compared to the inclined or vertical ones at shallow embedment depths. However, since the failure mechanism of the anchors in this condition is usually local (i.e., deep failure), the inclination does not play any role and the deep solutions (N^*_{c0}) may be generally applied. Similar results were reported by Yu et al.[29],: the inclination of the plate anchor reduces the N_c value at shallow depths for heavily weighted clay, which makes the anchor behave similarly as under attached conditions.

4.2.2. Failure mechanisms

Fig. 9 and Fig. 10 show the displacement contours of circular and square anchors under different conditions with different inclination angles at very shallow and deep embedment ratios. The plotted contours correspond to a vertical cross-section along the vertical midplane of the anchor. For horizontal anchors, only one-quarter of the problem was modelled, whereas, for the inclined ones, the model corresponds to half of the problem, as previously mentioned in Fig. 2. As seen in Fig. 9, almost in all cases of shallowly embedded anchors, soil displacement extended all the way up to the ground surface. Mostly in all cases, the

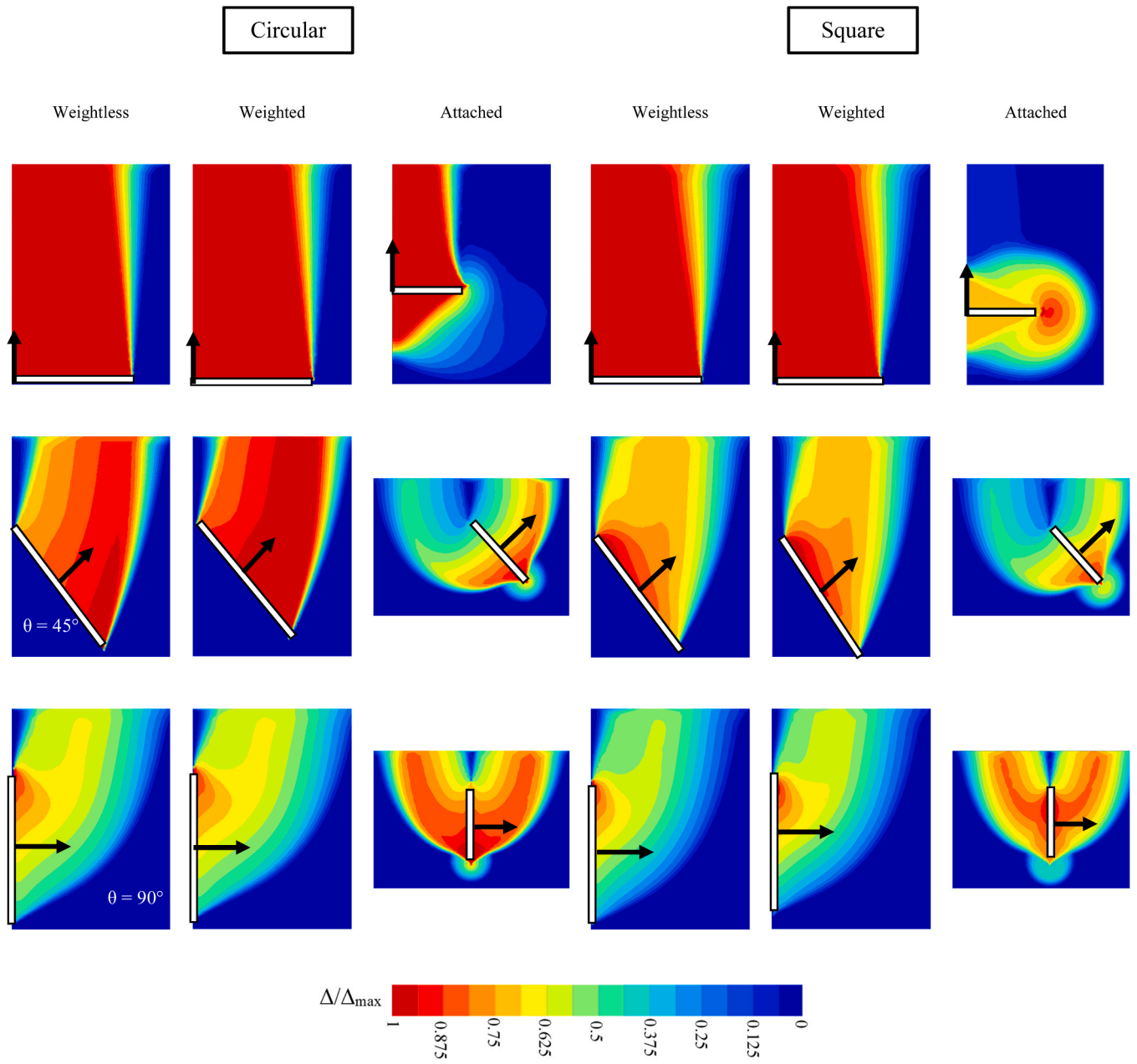

Fig. 9. Displacement contours of shallowly embedded anchors (embedment ratio of 1) at different inclination angles with different conditions.

unit weight of the soil did not have a significant influence on the failure mechanism of the anchor at a very shallow embedment ratio due to the minor level of overburden pressure. However, under attached conditions, the failure mechanism of the anchors experienced a significant change at a very shallow embedment ratio. While the shallow horizontal square anchor was on the verge of mobilising a deep failure mechanism, soil displacements above the circular anchor appear to be similar to those in the vented condition, with an obvious convex curvature directly above the anchor sides. Also, the attachment of the soil beneath the anchor caused a conical soil mass below it to move upward.

For the inclined anchors in the vented condition, the upward movement of the soil tends to change from a simple straight motion to a more curved and complex shape. This change becomes more noticeable as the angle of inclination (θ) increases from 45° to 90°. For the 45° inclined circular anchor, the failure mechanism is still shallow in the vented condition. In contrast, for the square anchor, soil movements are most significant just above the anchor and gradually decrease as they approach the ground surface. This suggests that the shallow failure mechanism for the square anchor at this embedment ratio has just begun to transition to a deeper mechanism.

For the inclined anchors in the attached condition, the failure mechanism followed a U-shape near the ground surface (passive wedge in front of the anchor and active wedge behind), displacing a significant volume of soil. The mobilised shear strength of the soil due to this type of failure mechanism was lower compared to the horizontal anchor. This is because one part of the soil behind the anchors (active wedge) experienced an inclined downward drag, while another part moved upward at an incline (passive wedge). Consequently, the resultant mobilised shear strength is reduced and lower values of N_c were obtained at shallow embedment depths, as previously observed in Fig. 8a and Fig. 8b.

Fig. 10 indicates the displacement contours of circular and square anchors under varying angles of mobilised deep failure mechanisms in weightless soil. The general shape of the deep failure mechanism appears to be the same for both circular and square anchors. However, as

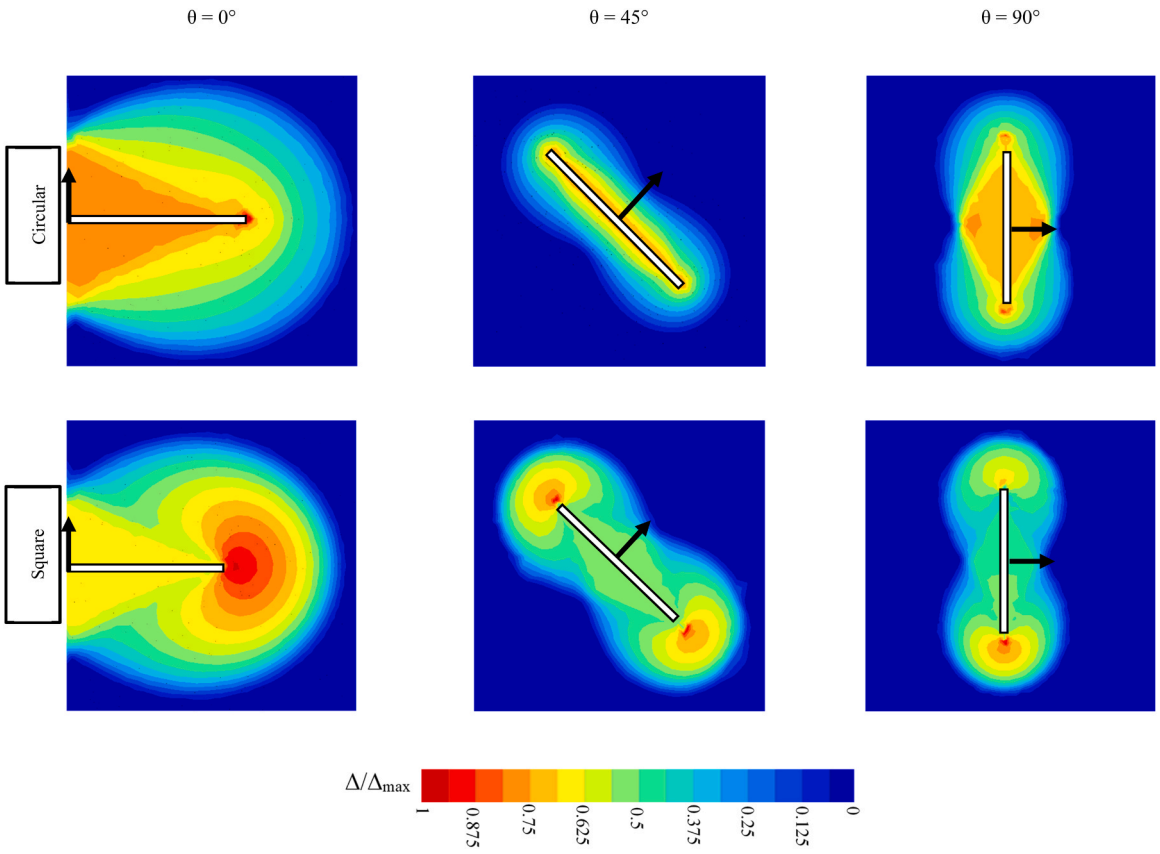

Fig. 10. Displacement contours of deeply embedded anchors at different inclination angles at an embedment ratio of 10.

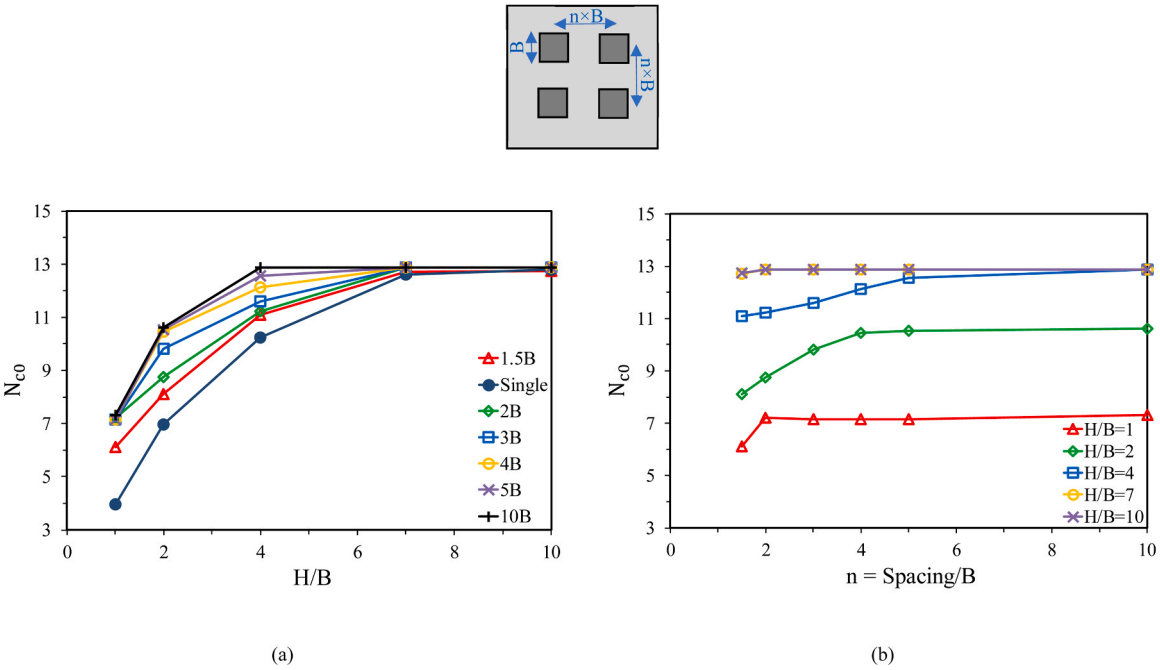

Fig. 11. Upper bound break-out capacity factor of grouped square anchors in weightless soil with vented condition.

observed, with the inclination of the anchor, the deep failure mechanism of both types of anchors merely changed orientation. This failure shape is independent of the initial stresses (soil weight and horizontal stresses) because the calculations correspond to limit analysis. Therefore, the limiting break-out factor is independent of the anchor inclination.

4.3. Anchor groups

The utilisation of shared anchors and anchor groups has emerged as a compelling prospect, for example, for floating wind turbine farms (e.g.,[2]) and therefore, this section analyses the performance of anchor

groups, specifically the optimum spacing between anchors. To investigate the effect of the spacing between anchors in a group on their break-out capacity, six different axis-to-axis spacings between a group of four anchors arranged in a square configuration in weightless soil were modelled numerically (Fig. 11). To reduce the computational cost and to exploit the symmetries of the problem, only a quarter of the group of anchors was modelled, i.e., only one anchor with the corresponding symmetry boundaries. The distance to the other boundaries and the finite element meshes follow what was mentioned in Section 2 for single anchors.

As can be seen in Fig. 11, for the shallowest embedded group of anchors ($H/B = 1$), all the anchors with different spacings had the same N_{c0}, except for the axis-to-axis spacing of 1.5B. This shows that in this case, the optimum spacing between anchors is around 2B. The optimum spacing is that at which each anchor separately reaches its shallow failure mode without interacting and reducing its individual capacity, i.e., no group effect. However, as the embedment ratio of the group of anchors increases, an increase in the optimum spacing is logically observed. This is mainly due to the change in the failure mechanism of the anchors at these embedment ratios, from very shallow to shallow or intermediate (Fig. 3), enlarging their area of influence. Therefore, the spacing must be greater in these cases to avoid group effects. Once the anchors reach the deep failure mechanism, the optimum spacing between anchors is around 1.5B because in this mode of failure, the slip lines are localised around the anchors as shown in Fig. 10.

5. Conclusions

This paper compares the vertical pull-out capacity of ultrathin and infinitely rigid square and circular anchors of equal area and depth in purely cohesive soils (i.e. clays in undrained conditions). The numerical results reveal, for the first time, that at very shallow depths, square anchors exhibit slightly higher efficiency due to their larger perimeter, which mobilises greater shear resistance. Specifically, at $H/B = 1$, square anchors have a 5 % higher vertical pull-out capacity. In contrast, at greater depths, circular anchors demonstrate superior efficiency, as their deep failure mechanism mobilises a larger failure surface area than that of square anchors, with a circular-to-square vertical pull-out capacity ratio of 1.04 (Table 2). The identification of this transitional efficiency behaviour between square and circular anchors with depth represents a novel contribution, providing practical guidance for the optimal selection of anchor shape depending on the installation depth.

Additionally, the deep failure mechanism of square anchors is explored for the first time through numerical simulations. It is observed that, as the anchor moves upwards, the soil moves around the anchor toward the square sides, rather than towards the corners, leading to a more confined failure mechanism compared to that of circular anchors (Fig. 7c).

The paper further investigates the influence of anchor inclination on their break-out factors under both vented and attached conditions. In vented conditions, inclined anchors demonstrate an increased break-out factor compared to horizontal anchors, as the inclination elongates the failure mechanism's contour. For attached conditions, the deep failure mechanism, which is independent of the anchor inclination and depth, was obtained in nearly all the cases ($H/B \geq 2$).

Finally, the effect of the spacing between anchors in a group on their break-out capacity was numerically analysed, specifically the optimum spacing between anchors to avoid interaction and reduction of the pull-out capacity (i.e. group effects). For very shallowly embedded anchors ($H/B=1$), a spacing of approximately 2B prevents group effects. As the depth increases, the failure mechanism extends laterally, necessitating larger spacings (around 4–5B for $H/B=2$–4) to avoid interaction. For deep embedded anchors, a spacing of around 1.5B is enough due to the localisation of the slip lines in the deep failure mechanism.

CRediT authorship contribution statement

Jorge Castro: Writing – review & editing, Writing – original draft, Supervision, Project administration, Methodology, Investigation, Funding acquisition, Conceptualization. **Marina Miranda:** Writing – review & editing, Supervision, Funding acquisition, Conceptualization. **Mohammadreza Jahanshahinowkandeh:** Writing – original draft, Visualization, Validation, Software, Investigation, Formal analysis, Data curation, Methodology, Conceptualization.

Declaration of Competing Interest

The authors declare that they have no known competing financial interests or personal relationships that could have appeared to influence the work reported in this paper.

Acknowledgements

This work is part of the R&D projects "Advanced methodology for foundation of critical structures in offshore wind farms (CREMA)" and "Fluid-structure-soil interaction for the development of offshore wind solutions at deep and very deep waters using taut or semi-taut mooring systems (INFLUET)" funded by MCIN/ AEI /10.13039/501100011033. This study also forms part of the ThinkInAzul programme and is supported by Ministerio de Ciencia e Innovación with funding from European Union NextGenerationEU (PRTR-C17.I1) and by Comunidad Autónoma de Cantabria through the project entitled: "Tools for the analysis of the interaction between the seabed and the foundations of offshore renewable energy structures (CIMA)".

Data availability

Data will be made available on request.

References

1. Cañizal F, Castro J, Cañizal J, Sagaseta C. Pull-Out capacity and failure mechanisms of strip anchors in clay. *Energies*. 2020;13(15):3853. https://doi.org/10.3390/en13153853.
2. Cerfontaine B, Gourvenec SM, White DJ. *Specificities of floating offshore wind turbines for risk and safety evaluation of anchoring systems. Geotech. Eng. Challenges to Meet Curr. Emerg. Needs Soc.* London: CRC Press; 2024:154–166.
3. Cheng X, Wang P, Li N, Liu Z, Zhou Y. Predicting the cyclic behaviour of suction anchors based on a stiffness degradation model for soft clays. *Comput Geotech*. 2020;122, 103552. https://doi.org/10.1016/j.compgeo.2020.103552.
4. Das BM. Model tests for uplift capacity of foundations in clay. *Soils Found*. 1978;18(2):17–24. https://doi.org/10.3208/sandf1972.18.2_17.
5. Fanning J, Sivakumar V, Nanda S, et al. Pullout capacity of single and biwing anchors in a soft clay deposit: model investigation in a centrifuge and FEM predictions. *J Geotech Geoenviron Eng*. 2023;149(7). https://doi.org/10.1061/JGGEFK.GTENG-10636.
6. Gaudin C, O'Loughlin CD, Hossain MS, Zimmerman EH. *The performance of dynamically embedded anchors in calcareous silt. Proc. Int. Conf. Offshore Mech. Arct. Eng. - OMAE.* American Society of Mechanical Engineers; 2013.
7. Gaudin C, O'Loughlin CD, Randolph MF, Lowmass AC. Influence of the installation process on the performance of suction embedded plate anchors. *Géotechnique*. 2006;56(6):381–391. https://doi.org/10.1680/geot.2006.56.6.381.
8. Giampa JR, Bradshaw AS, Gerkus H, Gilbert RB, Gavin KG, Sivakumar V. The effect of shape on the pull-out capacity of shallow plate anchors in sand. *Géotechnique*. 2019;69(4):355–363. https://doi.org/10.1680/jgeot.17.P.269.
9. Han C, Tong Y, Liu J. The performance of the dynamically installed plate anchor in sand and silt. *Ocean Eng*. 2023;267, 113274. https://doi.org/10.1016/j.oceaneng.2022.113274.
10. He P, Fenton GA, Griffiths DV. Pullout capacity of strip anchors in spatially variable soil. I: clay. *J Geotech Geoenviron Eng*. 2024;150(11). https://doi.org/10.1061/JGGEFK.GTENG-12574.
11. Jesmani M, Kamalzare M, Nazari M. Numerical study of behavior of anchor plates in clayey soils. *Int J Geomech*. 2013;13(5):502–513. https://doi.org/10.1061/(ASCE)GM.1943-5622.0000236.
12. Kwa KA, White DJ. Numerical modelling of plate anchors under sustained load: the enhancement of capacity from consolidation. *Comput Geotech*. 2023;158, 105367. https://doi.org/10.1016/j.compgeo.2023.105367.
13. Liu J, Lu L, Hu Y. Keying behavior of gravity installed plate anchor in clay. *Ocean Eng*. 2016;114:10–24. https://doi.org/10.1016/j.oceaneng.2016.01.018.

14. Martin CM. Undrained collapse of a shallow plane-strain trapdoor. *Géotechnique*. 2009;59(10):855–863. https://doi.org/10.1680/geot.8.T.023.
15. Martin C, Randolph M. Applications of the lower and upper bound theorems of plasticity to collapse of circular foundations. *th Int Conf Int Assoc Comput Methods Adv Geomech*. 2001;(10):1417–1428.
16. Merifield RS, Lyamin AV, Sloan SW. Three-dimensional lower-bound solutions for the stability of plate anchors in sand. *Géotechnique*. 2006;56(2):123–132. https://doi.org/10.1680/geot.2006.56.2.123.
17. Merifield RS, Lyamin AV, Sloan SW, Yu HS. Three-Dimensional lower bound solutions for stability of plate anchors in clay. *J Geotech Geoenviron Eng*. 2003;129(3):243–253. https://doi.org/10.1061/(ASCE)1090-0241(2003)129:3(243).
18. Merifield RS, Sloan SW, Yu HS. Stability of plate anchors in undrained clay. *Géotechnique*. 2001;51(2):141–153. https://doi.org/10.1680/geot.2001.51.2.141.
19. Murray EJ, Geddes JD. Uplift of anchor plates in sand. *J Geotech Eng*. 1987;113(3):202–215. https://doi.org/10.1061/(ASCE)0733-9410(1987)113:3(202).
20. O'Loughlin CD, Blake AP, Gaudin C. Towards a simple design procedure for dynamically embedded plate anchors. *Géotechnique*. 2016;66(9):741–753. https://doi.org/10.1680/jgeot.15.P.209.
21. Optum Computational Engineering. OptumG3: Program for Geotechnical Finite Element Analysis. ⟨www.optumce.com⟩; 2021.
22. Ovesen N. "Centrifuge tests of uplift capacity of anchors." *10thinternational. Conf Soil Mech Found Eng*. 1981;10(1):717–722.
23. Randolph MF. *Des Anchor Syst Deep Water Soft Sediment*. 2020:1–28.
24. Randolph M, Gourvenec S. *Offshore geotechnical engineering*. CRC Press; 2017.
25. Song Z, Hu Y, Randolph MF. Numerical simulation of vertical pullout of plate anchors in clay. *J Geotech Geoenviron Eng*. 2008;134(6):866–875. https://doi.org/10.1061/(ASCE)1090-0241(2008)134:6(866).
26. Vesić AS. Breakout resistance of objects embedded in ocean bottom. *J Soil Mech Found Div*. 1971;97(9):1183–1205. https://doi.org/10.1061/JSFEAQ.0001659.
27. Wang D, Hu Y, Randolph MF. Three-Dimensional large deformation Finite-Element analysis of plate anchors in uniform clay. *J Geotech Geoenviron Eng*. 2010;136(2):355–365. https://doi.org/10.1061/(ASCE)GT.1943-5606.0000210.
28. Wang C, O'Loughlin CD, Bransby MF, et al. Permeable plate anchors: accelerating capacity gain in soft clay. *J Geotech Geoenviron Eng*. 2024;150(1). https://doi.org/10.1061/JGGEFK.GTENG-11577.
29. Yu L, Liu J, Kong X-J, Hu Y. Numerical study on plate anchor stability in clay. *Géotechnique*. 2011;61(3):235–246. https://doi.org/10.1680/geot.8.P.071.